RSC Advances

ROYAL SOCIETY OF CHEMISTRY

www.rsc.org/advances

Two structural phase transitions are observed at 0.9 and 3.2 Gpa in acetamide using in-situ synchrotron X-ray diffraction (XRD) and Raman scattering techniques.

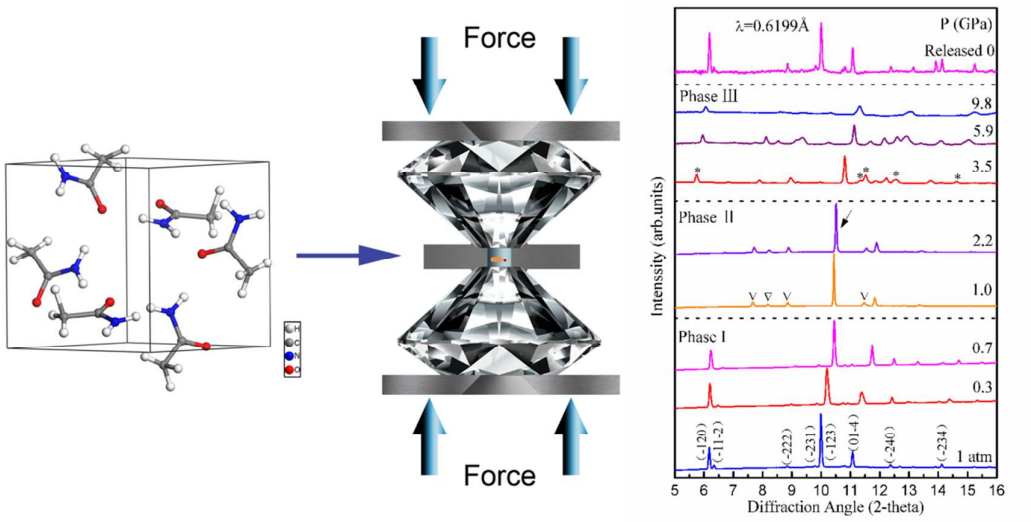

Journal Name

ARTICLE

Pressure-Induced Phase Transition in Hydrogen-Bonded Molecular Crystal Acetamide: Combined Raman Scattering and X-ray Diffraction Study

Received 00th January 20xx,
Accepted 00th January 20xx

DOI: 10.1039/x0xx00000x

www.rsc.org/

Lei Kang,[a] Kai Wang,[*a] Shourui Li,[a] Xiaodong Li[b] and Bo Zou[*a]

The structural and vibrational properties of acetamide under high pressure were probed by *in-situ* synchrotron X-ray diffraction (XRD) and Raman scattering up to ~ 10 GPa. Two structural phase transitions are observed at 0.9 and 3.2 GPa, evidenced by the obvious changes in Raman spectra as well as the discontinuities of peak positions versus pressure. The phase transitions are further confirmed by the significant changes of XRD patterns. The two phase transitions are proposed to originate from the rearrangements of hydrogen-bonded networks, deduced by the redistribution of intensities and positions of N-H vibrations. Detailed analysis of XRD patterns indicates that the first high-pressure phase (phase II) possesses a monoclinic structure with a possible space group of *C*2/*c*. Moreover, the phase transitions are reversible since the diffraction pattern returns to its initial state upon total decompression. The detailed mechanisms for these phase transitions, the cooperativity of different intermolecular interactions, as well as the high-pressure behaviors of hydrogen bonds are presented and discussed.

1. Introduction

Over the past decades, people have devoted considerable efforts into designing, synthesizing, and characterization of molecular crystals due to their industrial applications as well as fundamental importance.[1-3] The intermolecular interactions (hydrogen bonding, electrostatic interaction, π-π stacking, and van der Waals force, etc.), play vital roles in determining the physical and chemical properties of molecular crystals.[4-7] Especially, hydrogen bond is the most extensively studied intermolecular interaction because of its wide existence in biological, organic and inorganic materials.[8-10] The thorough knowledge of intermolecular interactions and their cooperation is a prerequisite of controlling molecular materials, including molecular self-assembly,[11] molecular recognition[12] and host-guest chemistry[13]. This makes it urgent to develop new methods to monitor their intrinsic properties from different perspectives.

As a fundamental thermodynamic parameter, pressure is extensively used to develop a comprehensive understanding of material properties and create new materials in chemistry, physics, and geoscience, through precise tuning interatomic distances, potentials, and thus electronic structures. Furthermore, compared with covalent interactions, the intermolecular interactions are so weak that their distances and strengths can be controlled easily by external pressure. Pressure can also help us to discover and synthesize new materials which are not accessible under atmospheric conditions, such as stable $NaCl_3$, Na_3Cl compounds and superconductive of sulfur hydride systems.[14,15]

Recently, pressure has proven itself as a powerful tool for investigating hydrogen-bonded molecular crystals, since slight variations in hydrogen bonds induced by compression can result in large rearrangements in crystal structures.[16,17] Besides, compared with the strength of covalent bond (150-400 kJ/mol) in molecules, hydrogen bonding interactions are far weaker (8-50 kJ/mol) and also a short-range force, so the geometry parameters of hydrogen bonds (e.g., bond strength, bond length, bond angle) can be easily altered by external force.[18] A lot of structural transitions in hydrogen-bonded crystals induced by pressure have been reported.[19-28] During phase transitions, large changes can be observed in hydrogen bonds, including break and formation,[23-25] distortion.[26] For example, the occurrence of the first phase transition in urea at 0.48 GPa, and then three transitions at about 0.6, 2.8, and 7.2 GPa, respectively.[27,28] During the phase transitions of urea, they found that one of the four hydrogen bonds broken, and interestingly, the capacity of the H-acceptor carbonyl oxygen restored when pressure reached 2.8 GPa.[24] Witold Zieliński *et al*.[16] performed high-pressure investigation on benzimidazole polymorphs, two phase transitions was found at 0.26 and 2.26 GPa, which were primarily driven by collapse of voids between NH···N′ bonded chains. However, there is still relatively limited research on hydrogen-bonded structures at high pressures, further high-pressure studies are needed to provide us more insight into hydrogen bond and its cooperation with other intermolecular interactions.

[a] *State Key Laboratory of Superhard Materials, Jilin University, Changchun 130012, China. Email: zoubo@jlu.edu.cn; kaiwang@jlu.edu.cn*
[b] *Beijing Synchrotron Radiation Laboratory, Institute of High Energy Physics, Chinese Academy of Sciences, Beijing 100039, China*
† Electronic Supplementary Information (ESI) available: The summarized phases of acetamide at different pressures and room temperature. See DOI: 10.1039/x0xx00000x

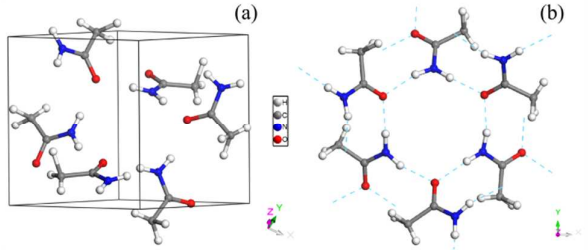

Fig. 1 Crystal structure and hydrogen-bonded networks of acetamide at ambient condition. (a) crystal structure; (b) hydrogen-bonded networks. Hydrogen bonds are marked as dashed lines.

Acetamide is a representative compound for the amide linkage in peptides and proteins with a simple hydrogen-bonded structure.[29] Acetamide can serve as a model system for studying complex intramolecular and intermolecular hydrogen bonding interactions in biologically systems such as peptides and proteins. Under ambient conditions, acetamide possesses two crystal forms, the stable rhombohedral *R*3*c* phase[30,31] and the metastable orthorhombic *Pccn* one[32]. In this study, the material used is the stable rhombohedral form, which is confirmed by X-ray diffraction measurement. It has space group *R*3*c* with Z = 18, the parameters of unit cell are $a = b =$ 11.526(5) Å, c = 13.589(5) Å, V = 1563.42 Å^3.[33] The crystal structure and hydrogen-bonded networks are shown in Fig. 1. Each acetamide molecule provides two hydrogen bond acceptors and two donors, forming four N-H···O hydrogen bonds with other molecules. Consequently, the stability of acetamide crystal structure is mainly governed by the balance between hydrogen bonding and van der Waals interactions. Bridgman[34,35] has chosen acetamide as a model material for his systematic high-pressure research, by means of volume measurements. He found the first transition at 0.59 GPa (293 K) with a decrease in volume of 1.85 cm^3/mol, followed by two transitions at 1.8 and 2.2 GPa (323 K), respectively. Subsequently, Hamann *et al.*[36] investigated the high-pressure behaviors of N-H stretching modes in acetamide in the range of 0-4.0 GPa. Fabbiani *et al.*[37] also studied acetamide using high-pressure crystallization techniques, the structure of the obtained single-crystal at 0.8 GPa was indexed to a monoclinic structure with space group of $P2_1/n$. The new high-pressure phase is suggested to be Bridgman's high-pressure at 0.59 GPa based on the similar density increase. As is known to all, the pressure effect is often different for single crystal and for powder crystal. For example, there is no structural transitions observed up to 4.0 GPa for single-crystal paracetamol, however, the powder samples of paracetamol phase I converted partially into phase II at lower pressures.[38,39] Single-crystal and powder experiments can complement each other when investigating the properties of material under various extreme conditions. It is therefore rather significant to study the behaviors of acetamide with powder crystal, which allows for a more in-depth understanding of the structure and stability. Besides, the P/T phase diagram of acetamide reported previously was limited to 5 GPa and the vibrational spectroscopic behaviors were not presented in detail, a detailed structural and vibrational spectroscopy investigation of acetamide through combining synchrotron X-ray diffraction and Raman scattering is necessary. *In-situ* synchrotron X-ray diffraction measurement is powerful to probe structural information under high pressure conditions. Raman scattering is sensitive to variations of hydrogen bonds and lattice vibrations. In this study, we report a comprehensive investigation of acetamide under high pressure by using X-ray diffraction and Raman scattering techniques up to ~ 10 GPa. The mechanism for the phase transitions, behavior of hydrogen bonds and crystal structures are proposed. This work can be helpful for further understanding the nature of hydrogen bonds as well as the stability of hydrogen-bonded structures.

2. Experimental Section

The powder sample in our experiments was obtained from Alfa Company (purity 99%) and used without further purification. *In-situ* high-pressure Raman spectroscopy and synchrotron X-ray diffraction measurements were conducted using symmetric diamond anvil cells (DACs) with 0.3 mm diamond culet in diameter. T301 steel was used as gasket, a hole with thickness of 0.04 mm and diameter of 0.13 mm served as the sample chamber. We used the standard ruby fluorescence method to calculate pressures in the sample chamber.[40] In Raman and XRD experiments, methanol - ethanol - water (16:3:1 in volume) was used as pressure transmitting medium (PTM). All of the measurements were carried out at room temperature.

In-situ high-pressure Raman spectra were recorded with Renishaw inVia Raman microscope using standard backscattering geometry. The visible 532 nm line with 10 mw laser power was used as excitation source. High-pressure angle-dispersive XRD (ADXRD) experiments were performed at 4W2 High Pressure Station of the Beijing Synchrotron Radiation Facility (BSRF) (wavelength 0.6199 Å, beam size 30 × 20 μm^2). Part of ADXRD experiments were carried out at the BL15U1 beamline of Shanghai Synchrotron Radiation Facility (SSRF) (wavelength 0.6199 Å, beam size 4 × 7 μm^2). Average acquisition time was 300 s. CeO_2 standard was used to calibrate geometric parameters before measurements. The diffraction data were recorded with a MAR345 imaging plate detector and the obtained XRD images were converted to one dimensional plots of intensity versus 2θ using FIT2D software.[41] High-pressure diffraction patterns were indexed and refined using Reflex module combined in the commercial Material Studio 5.5 program (Accelrys Inc.). The structural optimizations and phonon properties were performed using pseudopotential plane-wave method, based on density functional theory (DFT) implemented in the CASTEP code.[42] The local density approximation (LDA) with the Ceperley-Alder-Perdew-Zunger (CA-PZ) exchange-correlation function was used in the calculations.[43,44]

3. Results and discussion

Fig. 2(a) and 2(b) illustrate the calculated and observed Raman spectrum of acetamide at ambient pressure, respectively. The calculated spectrum of acetamide was calculated using DFT method and it shows very similar features to our experiment result. However, it is worth noting that some of the Raman modes in the calculated spectrum show obvious shift to lower frequencies compared with that of experimental results. This can be primarily explained that the calculation was based on T = 0 K rather than room temperature, which leads to the shrunken structure and slower movements of atoms. The factor group of acetamide is C_{3v} (3m). According to the

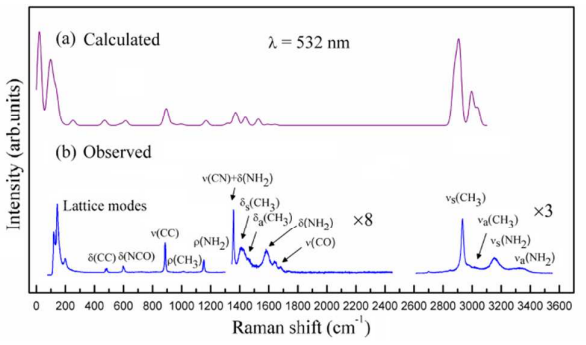

Fig. 2 (a) Calculated and (b) observed Raman spectra of acetamide at ambient conditions. The omitted spectral regions are due to the lack of spectroscopic features. All the assignments of the Raman modes are labeled above each band. The lines marked with ×8 and ×3 meaning the spectra are at a magnification of 8 and 3 times.

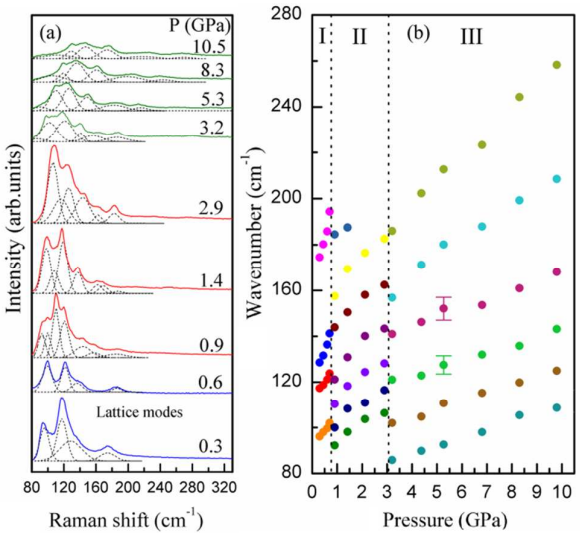

Fig. 3 (a) Selected Raman spectra of lattice modes in acetamide crystal at various pressures in the range of 80 - 330 cm^{-1}. Detailed decomposition of spectra are drawn for clarify. (b) Dependence of peak positions in lattice region versus pressure. The vertical dashed lines mean the boundaries of different phases.

factor group theory, the mechanical representation of this symmetry is

$$M = 27A_1 + 27A_2 + 54E \quad (1)$$

of which there are 2 acoustic modes

$$\Gamma_{acoustic} = A_1 + E \quad (2)$$

and 106 optic modes

$$\Gamma_{optic} = 26A_1 + 27A_2 + 53E \quad (3)$$

Based on the Raman selection rules, the A_2 modes are neither Infrared nor Raman active and the Raman active modes are $26A_1$ + 53E. But some of the modes could not be observed in our measurements because of weak intensities. Assignments of the Raman modes are based on the calculation and literatures.[29,45-46] The observed Raman spectrum can be divided into two regions, lattice modes region and internal modes region. Lattice modes involve relative movements among molecules or ions, while vibrations relate to molecular deformation are assigned to internal modes.

The evolutions of Raman spectra of acetamide crystal in the frequency regions 80 - 330, 400 - 1800, and 2800 - 3500 cm^{-1} at various pressures up to ~ 10.5 GPa are presented in Fig. 3(a), 4(a), and 5(a), respectively. Obvious variations (e.g., emergence of new modes, splitting of internal mode, disappearance of original modes) occur in the Raman spectra both in lattice and internal regions at 0.9 GPa, indicative of a pressure-induced phase transition (phase I → phase II). As pressure increasing, another structural transition (phase II → phase III) is identified at 3.2 GPa by the abrupt changes of Raman spectra. Because the sensitivity of phonons to pressure depends on crystal structures characteristics. The pressure dependence of the Raman modes are plotted, which are presented in Fig. 3(b), 4(b), and 5(b), as one can see, some modes show significant discontinuities at 0.9 and 3.2 GPa, which is consistent with the changes in Raman spectra. The phase III is found to be stable up to 10.5 GPa (the highest pressure in our experiment) with no further obvious changes in Raman spectra. Although little information is available about the high-pressure crystal structure of acetamide from Raman data, the observed Raman changes can provide us information about local structure, chemical bonding, which can offer insight into the phase transitions.

The Raman lattice modes, which involve collective motions of all atoms in the unit cell, are very sensitive to external pressure due to the weak intermolecular interaction.[47] As for acetamide, based on the literature,[29,45-46] we assign the modes below 200 cm^{-1} as lattice modes. As shown in Fig. 3(a), four lattice modes (95, 118, 131, and 174 cm^{-1}) are observed at 0.3 GPa. With increasing pressure, lattice modes exhibit normal blue shifts, however, with different shift rates. The observed blue shift for lattice modes is due to the reduction of intermolecular distances induced by external pressure, resulting in the increased interactions among adjacent molecules.[48,49] When pressure is increased to 0.9 GPa, remarkable changes in Raman patterns are observed. A new set of Raman pattern appears, which shows different spectra features both in positions, intensities, and profiles of Raman peaks. The appearance of new Raman spectrum suggests a structural transition from phase I to the high-pressure phase II at 0.9 GPa. With further compression to 3.2 GPa, another new set of Raman spectrum are observed with great reduction in the intensities of the new lattice modes, which indicates the second structural transition from phase II to the high-pressure phase III. No obvious discontinuous changes are detected at higher pressures above 3.2 GPa, suggesting the phase III is stable up to 10.5 GPa. Fig. 3(b) displays the plots of peak positions of lattice modes versus pressure in the pressure range of 0-10.5 GPa, obvious discontinuities can be observed at 0.9 and 3.2 GPa, which gives further evidence of the phase transitions. Furthermore, the pressure coefficients of lattice modes show obvious decrease in high-pressure phases (phase II, phase III) compared with that of ambient phase (phase I), which

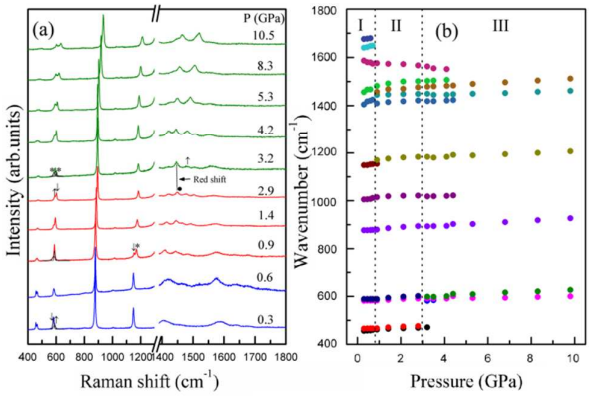

Fig. 4 (a) Selected Raman spectra of internal modes in acetamide crystal at various pressures in the range of 400 - 1800 cm^{-1}. Detailed decomposition of spectra are drawn for clarify. (b) Dependence of peak positions in internal region versus pressure. The vertical dashed lines mean the boundaries of different phases. The peaks marked by asterisks are the new peaks of high-pressure phases, and the peaks marked by up-facing and down-facing arrows represent their increasing and decreasing intensities with increasing pressure.

indicates the high-pressure phases of acetamide adopt more compact molecular packing, and therefore are more difficult to be compressed. The evolution of Raman lattice modes is regard as an effective probe of structural transitions. The significant changes observed in lattice region of Raman spectra indicate that there are two pressure-induced phase transitions at 0.9 and 3.2 GPa, respectively.

Analysis of Raman internal modes can provide fundamental information about the local changes of chemical environment around specific groups.[23] Fig. 4(a) displays selected Raman spectra in the range of 400 - 1800 cm^{-1}. With increasing pressure, most of internal modes shift gradually toward higher frequencies due to the decrease in bond lengths and increase in effective force constants.[50] However, remarkable changes are observed at 0.9 GPa. For example, the two modes marked by arrows (0.3 GPa) around 582 cm^{-1} related to the deformation of N-C=O show obvious variation in intensity. The mode assigned to rocking band of NH_2 at 1148 cm^{-1} reveals splitting, and the new peak marked by an asterisk gradually increases its intensity with the increasing pressure. Meanwhile, the original NH_2 rocking mode (marked by a down-facing arrow) suddenly decreases its intensity, and disappears at 1.4 GPa. The splitting of internal modes in Raman peaks can be regarded as an indication of a lower molecular and/or crystal symmetry as well as variations of the chemical environment due to the structural transition.[51] When pressure rises up to 3.2 GPa, two new modes appear marked by asterisks at around 600 cm^{-1}. The mode marked by a down-facing arrow at 2.9 GPa loses its intensity, while the mode marked by a up-facing arrow becomes the strongest one among the three modes. These changes indicate the chemical environment changes of atomic groups. What is more, the mode marked by a up-facing arrow around 1450 cm^{-1} gradually becomes stronger above 3.2 GPa. It is worth noting that the mode marked by a solid circle shows red shift at 3.2 GPa, which can be explained as the increased bond length and smaller chemical force constant induced by pressure.[50] The evolution of the internal modes versus pressure in the range of 400-1800 cm^{-1} is depicted in Fig. 4(b), most of the internal modes show increasing frequencies when pressure is increased, and discontinuities are observed at 0.9 and 3.2 GPa, which is consistent with the changes in Raman spectra, suggesting the structural changes. However, compared with lattice modes, the pressure coefficients of internal modes are very small. This can be explained that the covalent interactions are much stronger than intermolecular interactions, and therefore show lower compressibility.

Fig. 5(a) and 5(b) present the evolution of the Raman spectra and the corresponding pressure dependence of internal modes in the range of 2800-3500 cm^{-1}. The evolutions of N-H stretching vibrations are also play important roles in probing the structural changes in acetamide at high pressures. Three CH_3 stretching bands (2932, 2977, and 3025 cm^{-1}) and three NH_2 stretching bands (3155, 3311, and 3352 cm^{-1}) are observed at 0.3 GPa in Fig. 5(a). The mode centered at 3155 cm^{-1} is assigned as NH_2 symmetric stretching vibration, while the modes at 3311 cm^{-1} and 3352 cm^{-1} can be identified as NH_2 anti-symmetric stretching mode. The CH_3 stretching bands reveal no obvious changes except regular blue shifts due to the reduced bond lengths as well as increased bond strengths with increasing pressure up to 0.9 GPa. All these three N-H stretching modes exhibit red shifts with increasing pressure below 0.9 GPa, indicating the N-H···O hydrogen bonds in acetamide strengthened with increasing pressure.[52,53] For these hydrogen bonds, the electrostatic attractions are enhanced between O atoms and H atoms, leading to the elongated N-H distances and resulting in the red shifts of N-H stretching modes.[23] However, the intensities of the two CH_3 mode (2977 and 3025 cm^{-1} at 0.3 GPa) display abrupt increase at 0.9 GPa. Meanwhile, together with the disappearance of the original two N-H modes (3155, 3352 cm^{-1} at 0.3 GPa), two new

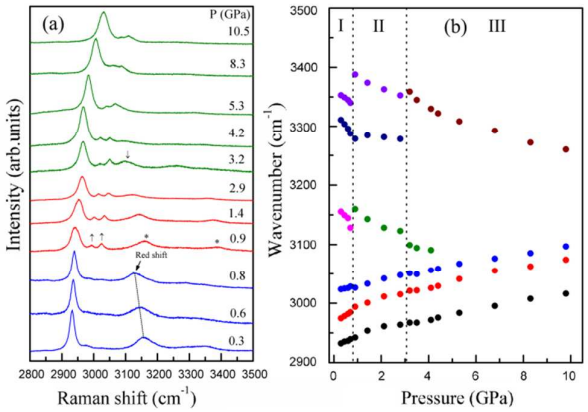

Fig. 5 (a) Selected Raman spectra of NH stretching vibration region in acetamide crystal at various pressures in the range of 2800 - 3500 cm^{-1}. (b) Dependence of peak positions in NH stretching vibrations region versus pressure. The vertical dashed lines mean the boundaries of different phases. The peaks marked by asterisks are the new peaks of high-pressure phases, and the peaks marked by up-facing and down-facing arrows represent their increasing and decreasing intensities with increasing pressure.

NH_2 stretching modes marked by asterisks at 3160 and 3388 cm^{-1} appear. These changes imply the reconstruction of hydrogen bonds under high pressure. Moreover, the positions and intensities of the N-H stretching modes display great changes at 0.9 GPa, suggesting the rearrangements of the hydrogen-bonded networks across the phase transition. With further compression to 3.2 GPa, the N-H mode at around 3311 cm^{-1} (0.3 GPa) disappears eventually, and the positions of the other two N-H stretching modes (3160, 3388 cm^{-1} at 0.9 GPa) changes obviously. For example, the mode centered at 3388 cm^{-1} reveals great blue shift, while the mode at 3160 shows red shift. Because all the NH_2 groups participate in the hydrogen-bonded networks, the obvious changes of the N-H mode positions as well as the disappearance of N-H modes confirm rearrangement of hydrogen-bonded networks. There are no obvious discontinuous changes detected except that the intensities of these modes become weaker when pressure is above 3.2 GPa in our experiment. The detailed information on the Raman peak positions as a function of pressure in this region is shown in Fig. 5(b). The discontinuities can be observed obviously at 0.9 and 3.2 GPa, further confirming the phase transitions. Variations of N-H stretching modes indicate that the structural transitions are probably accompanied by the rearrangements of hydrogen-bonded networks.

To confirm the phase transitions of acetamide at high pressures and obtain more structural information of the high-pressure phases, we carried out angle dispersive X-ray diffraction (ADXRD) measurement, which is believed to be a direct probe for structural transition. The representative ADXRD patterns of acetamide up to 9.8 GPa are summarized in Fig. 6. With increasing pressure, the diffraction peaks shift to high two-theta angles progressively. This can be explained as the reduced distances of crystal planes and the reduction of unit cell volume with the applied pressure. At ~ 1.0 GPa, many new peaks marked by hollow triangles appear, accompanied by the disappearance of original peaks of phase I, indicative of a structural transition to high-pressure phase II. Considering that the diffraction pattern at 1.0 GPa is very different from that at 0.7 GPa, we infer that the crystal structure has been reconstructed during the phase transition. Because single-crystal acetamide experiences a phase transition at a similar pressure (0.8 GPa),[37] we make a comparison between the high-pressure powder (in our experiment) and high-pressure single-crystal (high-pressure crystallization experiment) results at 2.2 GPa. The diffraction pattern at 2.2 GPa in the high-pressure single-crystal experiment is simulated based on the given structural information.[37] As shown in Fig. S1, the two diffraction patterns are totally different, neither the peak positions nor the peak intensities are consistent. This provides one more example that powder and single-crystal may have different behaviors at high pressures. With further pressure increasing, another phase transition can be proposed at ~ 3.5 GPa, evidenced by the emergence of new diffraction peaks marked with asterisks. At the same time, the intensity of the strongest peak of phase II at 2θ = 10.50° (marked by an arrow) reduces abruptly at 3.5 GPa. With further compression, there are no structural changes observed up to the highest pressure 9.8 GPa except the gradually normal reduced intensities of diffraction peaks. The decrease of intensities of diffraction peaks is due to the thinned sample at high pressures.

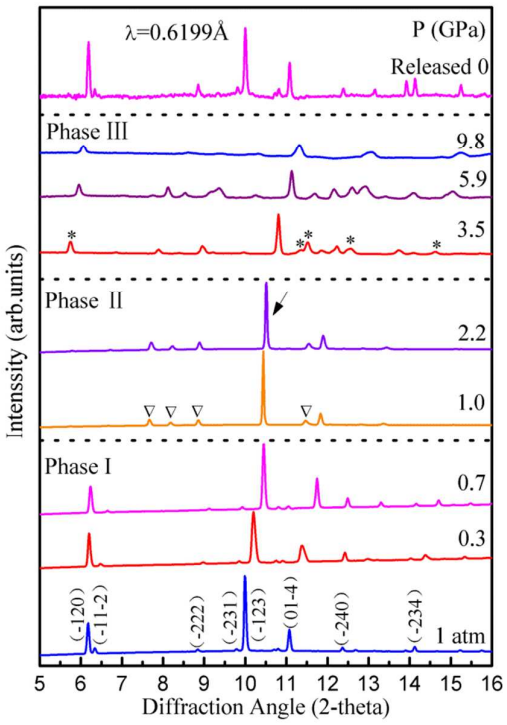

Fig. 6 Representative X-ray diffraction patterns of acetamide crystal at different pressures. The peaks marked by asterisks and rhombuses indicate the emergences of new phases.

Upon total release of pressure, the diffraction pattern matches very well with that of 1 atm, suggesting the reversibility of the phase transitions and the high-pressure phases can be completely recovered to its ambient crystal structure. However, the relative intensities among the diffraction peaks are slight different from the ambient pattern, which may be due to crystal orientation changes. Overall, the analysis of the high-pressure ADXRD data reveals that acetamide experiences two pressure-induced phase transitions at ~ 1.0 and ~ 3.5 GPa, which are within the same pressure region where Raman spectra show significant modifications. We also compare the diffraction patterns at 2.2 and 3.5 GPa with the existed phases of acetamide, as shown in Fig. S1. The diffraction patterns of the high-pressure phases (phase II and III) in our experiment show totally different features compared with the known phases (such as the metastable phase IV and the high-pressure crystallization phase V). The comparison results indicate that there are two new phases (polymorphs) obtained through high-pressure powder experiments.

We have performed refinements of the XRD patterns at 0.3 and 2.2 GPa to acquire the detailed structural information of ambient and high-pressure phases (as illustrated in Fig. 7). Rietveld refinement of the diffraction pattern at 0.3 GPa shows good agreement with *R*3*c* space group, generating lattice constants $a = b = 11.46(7)$ Å, $c = 13.18(5)$ Å, and unit cell volume $V = 1501.5(1)$ $Å^3$. The values of R factors are $R_P = 1.54\%$, $R_{WP} = 2.74\%$. The quality of least squares Refinements can be described by R-factors, the symbols P and W denote pattern and weighted, respectively. The smaller the value

(Rp, Rwp) is, the higher the quality of Refinements. The low R-factors indicate that the refinement result is acceptable and highly consistent with the lattice parameters of *R*3*c* reported previously. After the first transition at ~ 0.9 GPa, the ambient phase transforms to high-pressure phase II, a small number of diffraction points appear in the diffraction rings in the images, which may be due to the enlarged size of the crystalline grain during phase transition. The integrated intensities of diffraction peaks are inevitably affected by the distributions of points, which restrains any Rietveld refinement to acquire the accurate atomic positions of the high-pressure structure. We performed Pawley refinement to acquire lattice parameters of the high-pressure phase II. At 2.2 GPa, the crystal structure of phase II can be indexed and refined as monoclinic system with a possible *C*2/c space group, the lattice constants are a = 7.34(2) Å, b = 17.26(1) Å, c = 6.06(7) Å, β = 116.07(4)°, and unit cell volume V = 690.7(1) Å^3. The R-factors are R_P = 0.09%, R_{WP} = 0.25%. The values of R factors are very low, suggesting the acceptability of the refinement. The symmetry of the high-pressure phase II is lower than that of the ambient phase, which is consistent with the splitting of Raman internal mode at 0.9 GPa. The crystal structure of phase III cannot be determined because of the poor quality of diffraction data (lots of points in the diffraction rings). However, some information can be obtained based on the evolution of the diffraction patterns. As shown in Fig. 6, the profile of phase III at 3.5 GPa is similar to that of phase II at 2.2 GPa, which indicates the two high-pressure phases may have similar structures. In addition, it is suggested that the high-pressure phase III probably possesses much lower symmetry compared with phase II due to the appearance of extra diffraction peaks. Because the X-ray diffraction of light atoms is very weak (such as hydrogen atom and carbon atom), further neutron diffraction and single-crystal studies are needed to gain precious atomic positions of the high-pressure structures.

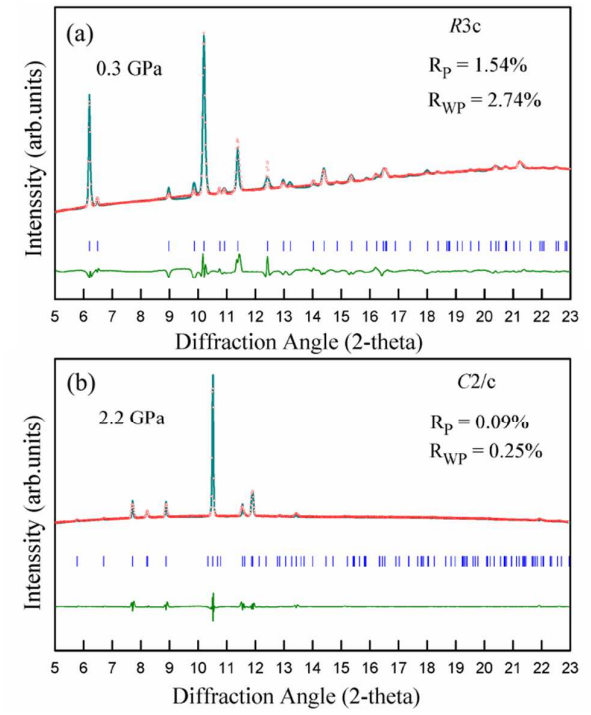

Fig. 7 Refinements of the diffraction profiles of high-pressure phases of acetamide at (a) 0.3 GPa, (b) 2.2 GPa, respectively. The olive lines show the difference between the observed (red circles) and the simulated (dark cyan lines) profiles and the vertical blue bars indicate the peak positions.

Formamide and acetamide are the first two compounds in amide system. It is worthwhile to compare the present results with the pressure-induced phase transitions in formamide. Formamide becomes solid state at about 0.5 GPa, and there is a structural transformation at 5.0 GPa.[54] During the phase transition, the pressure dependence of in-plane intermolecular stretching mode shows obvious slope change from 11.1 cm^{-1}/GPa to 19.2 cm^{-1}/GPa. When isochoric compression, formamide also transformates to a new phase at about 0.44 GPa due to the formation of new CH···O hydrogen bonds.[25] For acetamide, the first phase transition is at about 0.9 GPa, which is much higher than the first solid transition pressure (0.5 GPa) of formamide, this is due to the different structures. Formamide is built of N-H···O hydrogen-bonded sheets, and only van der Waals interactions exist between the sheets, the average distance between the sheets is about 3.0 Å. However, acetamide is built of three-dimensional N-H···O hydrogen-bonded networks. Due to the large voids between the hydrogen-bonded sheets in formamide, upon compression, the distortion of its structure should be easier compared with acetamides. Thus, lower pressure is expected to induce phase transition for formamide.

Based on the experimental results and the knowledge of the crystal structures, we propose mechanism for the pressure-induced structural transitions. Under ambient conditions, hydrogen bonding and van der Waals forces are two dominant interactions within acetamide to keep the structural stability. The structural transformation can be explained by the disturbed balance between the two factors. With pressure is increasing, the distances between the adjacent molecules are expected to be reduced, leading to the enhanced van der Waals forces between neighboring acetamide molecules. Meanwhile, the hydrogen bonding interaction also gets enhanced due to the reduced length of hydrogen bonds under rising pressure. This process will make contributions to the total Gibbs free energy. With further compression, the acetamide crystal structures cannot support the increasing Gibbs free energy any longer. Thus, the sliding and/or rotation of acetamide molecules occurs, resulting in the rearrangement of hydrogen-bonded networks (such as reconstruction, torsion) to reduce the free energy. Consequently, phase transitions occur at various critical pressures (0.9, 3.2 GPa) for acetamide crystal.

The proposed mechanism for the phase transitions is in agreement with changes observed in Raman and X-ray diffraction results. The substantial variations of lattice modes as well as internal modes in Raman scattering at 0.9 and 3.2 GPa indicate phase transitions, which are further confirmed by the new diffraction profiles of phase II and III. Pawley refinement suggests the high-pressure phase II possesses lower space symmetry compared with the ambient

structure, which is consistent with the splitting of the Raman internal modes of phase II. Moreover, high pressure induces the rearrangements of hydrogen-bonded networks at 0.9 GPa, as indicated by the differences in intensities and positions of N-H stretching bands during the structural transition. Furthermore, the transition at 3.5 GPa observed in XRD patterns can also be supported by the redistribution of positions of NH_2 mode as well as some discontinuous Raman modes. From these experimental results, we can tentatively infer that hydrogen bonding interactions play a vital role in the observed pressure-induced structural transitions.

4. Conclusions

The vibrational and structural properties of acetamide are analyzed by *in-situ* high-pressure synchrotron ADXRD and Raman scattering up to ~ 10 GPa. Abrupt changes in Raman spectra as well as the pressure dependence of Raman modes indicate that there are two phase transitions at ~ 0.9 and ~ 3.2 GPa, which are further confirmed by *in-situ* XRD analysis. The phase transitions are attributed to the rearrangements of hydrogen-bonded networks. Moreover, the diffraction pattern returns to its initial state when external pressure is completed released. High-pressure studies on acetamide can present some insight into the properties of hydrogen bonds as well as the structural stability of hydrogen-bonded crystals under high pressure.

Acknowledgements

This work is supported by NSFC (Nos. 91227202, and 11204101), RFDP (No. 20120061130006). XRD measurement was performed at 4W2 beamline, Beijing Synchrotron Radiation Facility (BSRF) which is supported by Chinese Academy of Sciences (No. KJCX2-SW-N03, KJCX2-SW-N20). Portions of this work were carried out at the 15U1 beamline at the Shanghai Synchrotron Radiation Facility (SSRF).

Notes and references

1 E. A. Silinsh, *Organic Molecular Crystals*, Springer, Berlin, 1980.
2 A. I. Kitaigorodsky, *Molecular Crystals and Molecules*, Academic Press, New York, 1973.
3 G. R. Desiraju, *Crystal Engineering: The Design of Organic Solids*, Elsevier, Amsterdam, 1989.
4 C. B. Aakeröy and A. M. Beatty, *Aust. J. Chem.*, 2001, **54**, 409.
5 C. J. Pickard and R. J. Needs, *Nat. Mater.*, 2008, **7**, 775.
6 T. Steiner, *Angew. Chem. Int. Ed.*, 2002, **41**, 48.
7 C. Q. Sun, B. K. Tay, S. P. Lau, X. W. Sun, X. T. Zeng, S. Li, H. L. Bai, H. Liu, Z. H. Liu and E. Y. Jiang, *J. Appl. Phys.*, 2001, **90**, 2615.
8 A. Luzar and D. Chandler, *Nature*, 1996, **379**, 55.
9 D. Braga and F. Grepioni, *Acc. Chem. Res.*, 2000, **33**, 601.
10 G. A. Jeffrey and H. Maluszynska, *Int. J. Biol. Macromol.*, 1982, **4**, 173.
11 F. H. Beijer, H. Koojman, A. L. Spek, R. P. Sijbesma and E. W. Meijer, *Angew. Chem. Int. Ed.*, 1998, **37**, 75.
12 K. K. Frederick, M. S. Marlow, K. G. Valentine and A. J. Wand, *Nature*, 2007, **448**, 325.
13 D. Jiao, F. Biedermann, F. Tian and O. A. Scherman, *J. Am. Chem. Soc.*, 2010, **132**, 15734.
14 W. Zhang, A. R. Oganov, A. F. Goncharov, Q. Zhu, S. E. Boulfelfel, A. O. Lyakhov, E. Stavrou, M. Somayazulu, V. B. Prakapenka and Z. Konopkova, *Science*, 2013, **342**, 1502.
15 A. P. Drozdov, M. I. Eremets and I. A. Troyan, *arXiv:1412.0460*, 2014.
16 W. Zieliński and A. Katrusiak, *Cryst. Growth Des.*, 2012, **13**, 696.
17 A. Katrusiak, M. Szafranski and M. Podsiadlo, Chem. Commun., 2011, **47**, 2107.
18 E. V. Boldyreva, *J. Mol. Struct.*, 2004, **700**, 151.
19 H. Tomkowiak, A. Olejniczak and A. Katrusiak, *Cryst. Growth Des.*, 2012, **13**, 121.
20 S. Q. Jiang, X. L. Huang, D. F. Duan, S. K. Zheng, F. F. Li, X. Yang, Q. Zhou, B. B. Liu and T. Cui, *J. Phys. Chem. C*, 2014, **118**, 3236.
21 E. Katoh, H. Yamawaki, H. Fujihisa, M. Sakashita and K. Aoki, *Phys. Rev. B*, 2000, **61**, 119.
22 S. Hunter, A. J. Davidson, C. A. Morrison, C. R. Pulham, P. Richardson, M. J. Farrow, W. G. Marshall, A. R. Lennie and P. J. Gould, *J. Phys. Chem. C*, 2011, **115**, 18782.
23 Q. Li, S. Li, K. Wang, X. Li, J. Liu, B. Liu, G. Zou and B. Zou, *J. Chem. Phys.*, 2013, **138**, 214505.
24 A. Olejniczak, K. Ostrowska and A. Katrusiak, *J. Phys. Chem. C*, 2009, **113**, 15761.
25 R. Gajda, A. Katrusiak, *Cryst. Growth Des.*, 2011, **11**, 4768.
26 K. Wang, J. Liu, K. Yang, B. Liu and B. Zou, *J. Phys. Chem. C*, 2014, **118**, 8122.
27 F. J. Lamelas, Z. A. Dreger and Y. M. Gupta, *J. Phys. Chem. B*, 2005, **109**, 8206.
28 W. G. Marshall, D. J. Francis, *J. Appl. Crystallogr.*, 2002, **35**, 122.
29 E.Ganeshsrinivas, D. N. Sathyanarayana, K. Machida and Y. Miwa, *J. Mol. Struct-theochem*, 1996, **361**, 217.
30 G. A. Jeffrey, J. R. Ruble, R. K. McMullan, D. J. DeFrees, J. S. Binkley and J. A. Pople, *Acta Crystallogr.,Sect. B*, 1980, **36**, 2292.
31 F. Senti and D. Harker, *J. Am. Chem. Soc.*, 1940, **62**, 2008.
32 S. Watanabe, Y. Abe and R. Yoshizaki, *J. Phys. Soc. Jpn.*, 1986, **55**, 2400.
33 W. A. Denne and R. W. H. Small, *Acta Crystallogr., Sect. B*, 1971, **27**, 1094.
34 P. W. Bridgman, *Proc. Am. Acad. Arts Sci.*, 1938, **72**, 227.
35 P. W. Bridgman, *Proc. Am. Acad. Arts Sci.*, 1916, **52**, 91.
36 D. Hamann. Sefton and M. Linton. *Aust. J. Chem.*, 1976, **29**, 1644.
37 F. P. A. Fabbiani, D. R. Allan, W. G. Marshall, S. Parsons, C. R. Pulham and R. I. Smith, *J. Cryst. Growth*, 2005, **275** 185.
38 E. V. Boldyreva, T. P. Shakhtshneider, H. Ahsbahs, H. Sowa, and H. Uchtmann, *J. Therm. Anal. Calorim.*, 2002, **68,** 437.
39 E. V. Boldyreva, T. P. Shakhtshneider, M. A. Vasilchenko, H. Ahsbahs and H. Uchtmann, *Acta Crystallogr., Sect. B: Struct. Sci*, 2000, **56**, 299.
40 H. Mao, J.-A. Xu and P. Bell, *J. Geophys. Res.*, 1986, **91**, 4673.
41 A. P. Hammersley, S. O. Svensson, M. Hanfland, A. N. Fitch and D. Hausermann, *High Pressure Res.*, 1996, **14**, 235.
42 S. J. Clark, M. D. Segall, C. J. Pickard, P. J. Hasnip, M. J. Probert, K. Refson and M. C. Z. Payne, *Z. Kristallogr.*, 2005, **220**, 567.
43 D. M. Ceperley and B. J. Alder, *Phys. Rev. Lett.*, 1980, **45**, 566.
44 J. P. Perdew and A. Zunger, *Phys. Rev. B*, 1981, **23**, 5048.
45 S. T. King, *Spectrochimica Acta Part A*, 1972, **28**, 165.
46 R. Knudsen, O. Sala and Y. Hase, *J. Mol. Struct.*, 1994, **321**, 187.
47 K. Harvey and N. J. McQuaker, *Chem. Phys*., 1971, **55**, 4390.
48 J. A. Ciezak, T. A. Jenkins, Z. Liu and R. J. Hemley, *J. Phys. Chem. A*, 2007, **111**, 5.
49 T. R. Park, Z. A. Dreger and Y. M. Gupta, *J. Phys. Chem. B*, 2004, **108**, 3174.
50 A. Torabi, Y. Song and V. N. Staroverov, *J. Phys. Chem. C*, 2013, **117**, 2210.
51 Z. A. Dreger and Y. M. Gupta, *J. Phys. Chem. B*, 2007, **111**, 3893.
52 S. Hamann and M. Linton, *Aust. J. Chem.*, 1977, **30**, 2591.
53 J. Joseph and E. D. Jemmis, *J. Am. Chem. Soc.*, 2007, **129**, 4620.
54 H. Shimizu, K. Nagata and S. Sasaki, *J. Chem. Phys.*, 1988, **89**, 2743.